Available online at www.sciencedirect.com

ScienceDirect

journal homepage: www.elsevier.com/locate/he

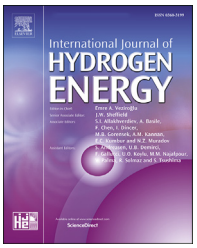

Perspective of interstitial hydrides of high-entropy alloys for vehicular hydrogen storage

Aaron Keith [a,b], *Claudia Zlotea* [b], *Petra Ágota Szilágyi* [c,*]

[a] *School of Engineering and Materials Science, Queen Mary University of London, Mile End Campus, E1 4NS, London, United Kingdom*

[b] *Université Paris Est Créteil, CNRS, ICMPE, UMR 7182, 2 rue Henri Dunant, 94320 Thiais, France*

[c] *University of Oslo, Centre for Materials and Nanotechnology (SMN) and Department of Chemistry, Kjemibygningen, Sem Sælands vei 26, 0371, Oslo, Norway*

HIGHLIGHTS

- The authors have collected what is perceived as the most vital parameters for hydrogen storage in HEAs for the first time.
- The valence electron count allows to incentivise the formation of the most favourable structure (BCC alloy that distorts into a *pseudo*-FCC hydride).
- The hydrogen affinity assesses the ability of an alloy to form a stable hydride.
- The affinity value is dependent on stoichiometric and elemental contributions.
- Random elemental distribution is highlighted as vital for reliable storage performances.

ARTICLE INFO

Article history:
Received 29 August 2022
Received in revised form
27 December 2022
Accepted 12 January 2023
Available online xxx

Keywords:
Hydrogen storage
High-entropy alloy
Hydrogen affinity
Hydrogen vehicles

ABSTRACT

The transport sector is an important source of CO_2 emissions worldwide, and a transition towards hydrogen-fuelled vehicles is a potential remedy. These vehicles require improvements in storage capacities, which can be realised by forming the interstitial hydrides of High-Entropy Alloys (HEAs) by synthesising single-phase hydrides with a randomised atomic distribution of the metal elements within these alloys. Not only is the randomness of elemental distribution in the hydride essential, so too is the affinity of the individual components towards hydride formation, which drastically improves the prospective storage. By evaluating the composition and properties of the best-performing hydride forming alloys, various parameters strongly influencing hydrogen capacities can be inferred. Herein, the state of literature regarding the parameters with the highest importance for hydrogen sorption in HEAs is discussed for the first time with particular focus on how they may be introduced to storage on-board vehicles.

* *Corresponding author.*
E-mail address: p.a.szilagyi@kjemi.uio.no (P.Á. Szilágyi).

https://doi.org/10.1016/j.ijhydene.2023.01.141

Introduction

Hydrogen in the transport sector

Globally, the transportation sector in 2019 was responsible for releasing 8.25 $GtCO_2$ into the atmosphere [1]. The 2019 British Department for Business, Energy, and Industrial Strategy's statistics detailing anthropogenic greenhouse-gas emissions paint a bleak picture, with 27% (some 120 $MtCO_2e$) of the greenhouse-gas produced for the entirety of the UK coming from the transport sector alone [2]. This constitutes the single largest sector emitting CO_2 in the UK, overtaking energy production for the first time in recorded history [2].

Despite the improvements in fuel efficiency for vehicles, leading to decreased CO_2 production per mile driven (with the fuel preference changing from petrol to diesel also a contributing factor) [3], the volume of CO_2 released into the atmosphere from transportation has remained at approximately the same level since the 1990s (between around 125–137 $MtCO_2$ per year) [4]. In fact, the rate at which the number of cars on the road has increased has consistently outpaced any technological advancements that reduce the emissions by fossil-fuel internal-combustion vehicles (FFICVs), negating the benefits of these advancements [3]. In order to realise a more sustainable and environmentally friendly future for the transportation sector, a transition away from the current paradigm is not only beneficial, but also a necessity.

To date, alternative technologies to FFICVs have mostly comprised battery electric vehicles (BEVs). However, the intrinsic problem of BEVs is that increasing driving range requires an exponential increase in the mass load [5]. As a result, BEVs are unsuitable for heavy-duty, long-range applications [5]. Therefore, for these applications (including aviation, maritime, and road-borne haulage) hydrogen is a key candidate to step away from FFICVs, however, how can this be realistically achieved?

Hydrogen storage

Storage targets

The US Department of Energy (DOE) has outlined targets for the gravimetric and volumetric hydrogen storage (*i.e.* uptake my weight and by volume, respectively) in light-duty vehicles, with the first milestone for storage capacity targets being a gravimetric storage capacity of 0.045 kg (H_2)/kg (storage system) (4.5 wt%), and a volumetric capacity of 0.030 kg L^{-1} (0.030 g cm^{-3}) with the temperature and pressure of storage between −40 and +60 °C and 5–12 bar, respectively [6]. The ultimate aim is to further increase this to 6.5 wt% and 0.050 g cm^{-3} [6]. This target is often considered the '*gold standard*' as it pertains to the criteria for germane hydrogen storage in the transportation sector. In a general sense, there are two broad categories of hydrogen-storage solutions; physical (tank-based) and chemical (materials based). Both of which offer benefits and drawbacks.

Physical storage

Currently there are three different approaches by which hydrogen can be physically stored: i) as a liquid at cryogenic temperatures (~20 K), ii) as a gas at elevated pressures (700 bar), or iii) in a hybrid system of the two [7]. All three physical-based methods allow the purity of the hydrogen to be guaranteed and favourable kinetics of hydrogen discharge. Refuelling times are, therefore, left unhampered. Physical storage offers a 100 wt% capacity of hydrogen in the internal system (excluding the container mass), hence a high gravimetric uptake is achieved.

However, these methods of storage are woefully inefficient from a volumetric perspective, impinging on the effectiveness of hydrogen storage in vehicles. This drawback is in no small part due to the logistical and economic demands of cryogenic cooling apparatus and/or compression. Physical storage, ignoring the safety concerns of up to 700 bar of a highly explosive and flammable gas being stored in vehicles travelling at high speeds, offers poor volumetric uptake regardless of the method. High-pressure storage offers a volumetric capacity of 5.6 MJ L^{-1}, and liquid-hydrogen storage which, while higher than high-pressure storage, also offers a low 10.1 MJ L^{-1} [7], which is a clear disadvantage when compared with the volumetric capacities of 34.2 MJ L^{-1} and 34.6 MJ L^{-1} offered by petrol and diesel, respectively [7]. A decrease in storage as drastic as this is not advantageous for wide-scale deployment, therefore, how can these shortcomings of the system be rectified?

Chemical storage

Chemical storage of hydrogen in so-called '*hydrogen carriers*' can offer a solution to the volumetric capacity issues of the physical-storage methods. There are a multitude of means by which hydrogen can be stored in solid or liquid carriers, many of which also result in an increased volumetric storage capacity. In principle, there are two categories of chemical storage based on the nature of the uptake: chemisorption and physisorption. Chemisorption may occur through direct covalent and/or metallic bonding in an (in-)organic carrier *e.g.* ammonia, $NaAlH_4$, or in BN-methyl cyclopentane [8]. This allows for a high gravimetric density of hydrogen – for example, 66.7 at.% (7.2 wt%) in MgH_2 [9], or 75 at.% (17.6 wt%) of hydrogen in ammonia – in stable compounds [10].

However, the desorption of hydrogen from these carriers often requires irreversible thermal decomposition of the carrier at high temperatures (upwards of ~200 °C) [11]. Therefore, the chemisorption of hydrogen in alternative chemical carriers could prove more advantageous, a compelling candidate for this can be found in the interstitial hydrides of metal alloys.

Interstitial hydrides

Interstitial hydrides are elemental or alloyed metals (typically, binary or ternary alloys, *e.g.* Pd [12], TiFe [13], $LaNi_5$ [14], PdAgAu [15]) wherein hydrogen has permeated into the interstices, the voids between the metal atoms of the lattice. The hydrogenation process begins with the adsorption of dihydrogen onto the surface of the metal, followed by homolytic dissociation into two hydrogen atoms, and finally the hydrogen permeates into the lattice to occupy the interstitial sites [16]. The molar uptake of hydrogen, measured as hydrogen atom-to-metal atom ratio (*H*/*M*), within these systems has been limited to $H/M = \sim 2$ [17].

However, the metals used are often prohibitively expensive and far too heavy for mobile applications (*e.g.*

Please cite this article as: Keith A et al., Perspective of interstitial hydrides of high-entropy alloys for vehicular hydrogen storage, International Journal of Hydrogen Energy, https://doi.org/10.1016/j.ijhydene.2023.01.141

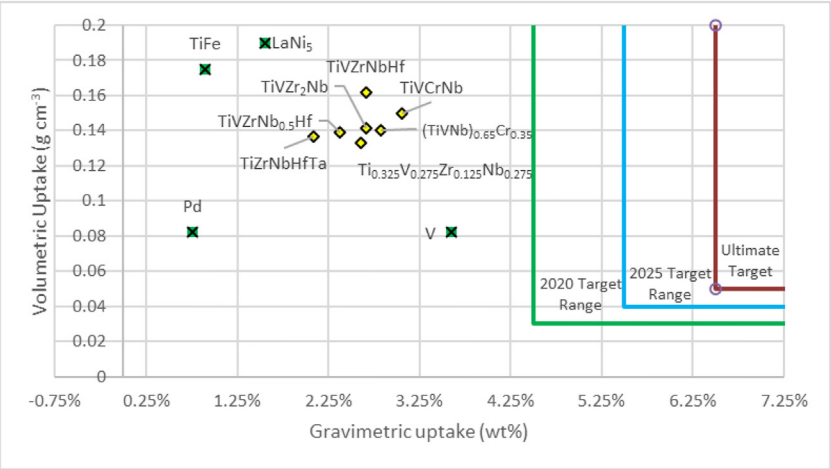

Fig. 1 – Volumetric uptake of HEAs (g cm^{-3}) *v* the gravimetric uptake (wt%) of given metals. The yellow diamonds are HEA hydrides, while the crossed, green squares show traditional interstitial hydrides [29]. The US DOE targets initially aim for a gravimetric uptake of 4.5 wt% and volumetric uptake of 0.030 g cm^{-3}, and to ultimately reach 6.5 wt% and 0.040 g cm^{-3} [6]. (For interpretation of the references to color/colour in this figure legend, the reader is referred to the Web version of this article.)

$LaNi_5$ = 432.37 g mol^{-1}). Furthermore, the constituent elements are generally scarce (*e.g.* La, Pd). Therefore, favouring the implementation of abundant and lightweight materials affording a higher hydrogen uptake could offer a route for effective deployment of interstitial hydrides as on-board vehicular hydrogen stores. One proposed candidate featuring all three characteristics are the interstitial hydrides of high-entropy alloys.

High-entropy alloys

High-Entropy Alloys (HEAs) are multicomponent alloys, comprised of four or more elements, in a strict sense in equal atomic proportions and of 5–35 at.% of the resultant alloy in a broader sense. These alloys most often form standard Hexagonal Close Packing (HCP), Body-Centred Cubic (BCC), and/or Face-Centred Cubic (FCC) lattices [18]. In addition, we also consider hexagonal C14-Laves (C14), or cubic C15-Laves (C15) crystal packing structures for intermetallic compounds [19,20]. Hence "*high entropy*" does not refer to the structure of the lattice, rather it denotes that the distribution of the atoms throughout the solid solution is practically random. HEAs have been researched extensively in relation to mechanical utilisation, as they offer substantial improvements with regard to various properties such as hardening [20], corrosion resistance [21,22], thermoelectric properties [23], electrocatalysis (including hydrogen evolution reactions) [24]. In addition, they may also be effectively employed as a solid hydrogen-storage material.

As stated previously, traditional metal alloys can lend themselves to be a suitable hydrogen store, and HEAs are no exception. Hydrogen storage in HEAs – as in traditional alloys - alloys is reversible, with some HEAs reporting a very high stability over cycling – one such alloy retaining 99% of the initial molar capacity over 1000 cycles [25]. In comparison to traditional alloys, HEAs can offer an equivalent, or higher, molar capacity, with the highest known reaching H/M = 2.5 [26]. This, compounded with the average molecular mass of HEAs being drastically lower thanks to the mass reduction from avoiding the usage of elements *e.g.* La or Pd in certain traditional interstitial hydrides and instead incorporating elements such as Ti or V, leads to a substantial increase in gravimetric storage, even when the volumetric storage for both may be the same (Fig. 1). That said, heavy constituent elements are still implemented in HEAs, albeit in proportions significantly lower than in that of traditional alloys – resulting in the same net decrease in molar mass.

For instance, if a comparison between the hydrides $Ti_{0.2}Zr_{0.2}Nb_{0.2}V_{0.2}Cr_{0.2}H_{1.21}$ (66.99 g mol^{-1}) and $LaNi_5H_{6.8}$ (432.37 g mol^{-1}) is drawn, the gravimetric uptake of 1.77 wt% for $Ti_{0.2}Zr_{0.2}Nb_{0.2}V_{0.2}Cr_{0.2}$ is a clear increase relative to the uptake of 1.56 wt% for $LaNi_5H_{6.8}$ and comes with a significantly reduced dependence on scarce, heavyweight elements (La) [27,28]. This disparity in gravimetric uptake occurs, even when the molar uptake for both the HEA relative to $LaNi_5$ are comparable – where H/M = 1.21 for the HEA and H/M = 1.13 for $LaNi_5$ [27,28]. Hypothetically, were TiZrNbVCr to have an identical molar uptake to $LaNi_5$, the gravimetric uptake would still be higher at 1.67 wt%. This is a very promising step towards the aims of the DOE targets, not least as HEAs can be formed of lighter materials, conferring them a great potential as hydrogen carriers for vehicular applications.

In order to evaluate the suitability of these novel materials for on-board storage and identify the most relevant *ab initio* design parameters affecting the uptake in HEAs, we summarise and discuss the current state of the literature below.

Current achievements in the field of research of high-entropy alloys

The potential of HEAs as hydrogen-storage materials has only recently started to raise attention within the scientific community. To the best of the authors' knowledge at the time of

Please cite this article as: Keith A et al., Perspective of interstitial hydrides of high-entropy alloys for vehicular hydrogen storage, International Journal of Hydrogen Energy, https://doi.org/10.1016/j.ijhydene.2023.01.141

writing, some 55 alloys/intermetallic compounds have been investigated for their performance as hydrogen stores (Table 1), with the majority of them being analysed since the beginning of 2020.

For HEAs whose hydrogen uptake has been measured, the alloys/intermetallics typically form FCC [26,27,40,43–45,49,50,54,55], BCC [17,26,27,31,34,37,38,40,42–46,48–51,54–56], or C14 [17,30,34,39,49,52] (either single phase or multiple phases of, see Table 1) lattices. Of these arrangements, it appears that the BCC structure is the most advantageous for high hydrogen uptake, as all of the alloys that outperform traditional interstitial hydrides, including the alloy with the highest molar uptake $H/M = 2.50$, form a BCC alloy that distorts into a BCT (Body-Centred Tetragonal) hydride which can be viewed as a slightly distorted FCC [26]. The highest molar uptake belongs to TiVZrNbHf and also comes with an impressive gravimetric capacity of 2.70 wt% [26]. This is a substantial increase in both the molar and gravimetric uptakes in comparison to $LaNi_5H_{6.8}$ (1.56 wt% and $H/M = 1.13$) [28].

To maximise uptake, it is logical to select the structure from the lattices most often afforded by HEAs or intermetallics which contains the maximum number of interstitial sites. A comparison of FCC, BCC, or C14 lattice types in terms of their theoretical maximum for hydrogen uptake is therefore reasonable. Of these three packing arrangements, BCC has the most interstitial sites – a total of 18 sites comprised of 12 tetrahedral, and 6 octahedral sites [57] – which can be simultaneously occupied in some cases [58]. However, not all interstitial sites can be occupied simultaneously by hydrogen: several well-known criteria already have been proposed for conventional alloys, including the available interstitial sites must have a spherical volume with the radius ≥0.4 Å [59] and the minimum distance between two hydrogen atoms is 2.1 Å under ambient conditions [60], though it has been shown recently that the latter may be violated [61]. The BCC alloys $Mg_{0.28}V_{0.28}Al_{0.19}Cr_{0.19}Ni_{0.06}$ and AlCrFeMnNiW, the latter of which is multi-phased with the major component being BCC [40], have low molar and gravimetric uptakes, ($Mg_{0.28}V_{0.28}Al_{0.19}Cr_{0.19}Ni_{0.06}$: $H/M = 0.15$, and 0.30 wt%; AlCrFeMnNiW: $H/M = 0.41$ and 0.61 wt%) [40,42]. Obviously, as also shown by the above results, the mere condition of a BCC alloy is not sufficient in and of itself to guarantee an elevated hydrogen uptake. This begs the question, why?

Hydrogen affinity

Griessen and Driessen proposed a semi-empirical model, which allows alloys to be assessed for their affinity to hydrogen [62]. Hydrogen affinity refers to the ability of an alloy to form an interstitial hydride and said model allows for its qualitative approximation from the enthalpy of solution at infinite dilution (ΔH_∞) and the enthalpy of formation of the concentrated hydride (ΔH_f) [62]. ΔH_f describes the heat change of a system due to interstitial hydride formation; ΔH_∞ describes the enthalpy of the dissolution of atomic hydrogen through the lattice. For the highest theoretical hydrogen affinity, both values require a large magnitude and negative sign if the hydride is to successfully form [32], *i.e.* strongly exothermic. When one – or both – of these processes are endothermic, the structure does not form the hydride and does not allow the dissolution and permeation of the absorbed hydrogen, hence the system is referred to as having a low hydrogen affinity [48]. A high affinity would lower the energy required to form the hydride, thus pushing the system in the direction of the DOE's storage targets [6].

It is necessary to understand which elements are the most advantageous for elevating hydrogen storage capacities in HEAs. In order to do this, analysing the individual classification of the chosen elements and their effects on hydrogen storage in these alloys needs to be understood.

Classification of metals in respect of hydrogen uptake

Traditional intermetallic alloys, that have been investigated for hydrogen uptake, follow the general formula AB_x, where element 'A' refers to, in general, an alkaline, early transition, actinide, lanthanide, or rare-earth metal, whereas element 'B' refers to a late transition metal (Table 2) [63]. A type metals have a stronger affinity towards hydrogen than B type [63]. As a design principle, therefore, in order to maximise hydrogen uptake, it is, advisable to maximise the utilisation of A type metals.

The values of ΔH_∞ and ΔH_f are found *via* the semi-empirical, computational analysis of the band structure of metals [62]. ΔH_f is calculated from considering the heats of formation of the hydride of the individual metals and ΔH_∞ is calculated by combining non-local and local effects that have an impact on the site the hydrogen atom occupies. An estimated value for ΔH_∞ and ΔH_f for an alloy can be achieved using the weighted average of the elements present in the alloy (Equations (1) and (2)).

$$\Delta H_\infty = \sum_{i=1}^{n} c_i \Delta H_{\infty i} \quad (1)$$

$$\Delta H_f = \sum_{i=1}^{n} c_i \Delta H_{f_i} \quad (2)$$

Equation (1): Evaluation of the enthalpy of solution at infinite dilution of an alloy where c_i is the stoichiometry of the ith element, and $\Delta H_{\infty(i)}$ is the enthalpy of solution at infinite dilution for the pure metal *i*. Equation (2): Evaluation of the enthalpy of formation of the concentrated hydride of an alloy, ΔH_f, where c_i is the stoichiometry of the ith element, and $\Delta H_{f(i)}$ is the enthalpy of formation of the concentrated hydride for the pure metal *i*.

With reference to the BCC alloys discussed above, the affinity values explain their hydrogen uptake values (Table 3). Looking specifically at the values for the previous examples (TiVZrNbHf, TiZrNbHfTa, $Mg_{0.28}V_{0.28}Al_{0.19}Cr_{0.19}Ni_{0.06}$, and AlCrFeMnNiW), the uptake increases with the decrease in ΔH_∞ and ΔH_f values. TiVZrNbHf ($\Delta H_\infty = -42.00$ kJ mol^{-1} and $\Delta H_f = -60.40$ kJ mol^{-1}) and TiZrNbHfTa ($\Delta H_\infty = -43.20$ kJ mol^{-1} and $\Delta H_f = -59.60$ kJ mol^{-1}) clearly favour the formation of the interstitial hydride, whereas $Mg_{0.28}V_{0.28}Al_{0.19}Cr_{0.19}Ni_{0.06}$ and AlCrFeMnNiW ($\Delta H_\infty = +17.05$ kJ mol^{-1} and $\Delta H_f = -22.87$ kJ mol^{-1}, $\Delta H_\infty = +38.00$ kJ mol^{-1} and $\Delta H_f = -0.67$ kJ mol^{-1} respectively) do not. Overall, the larger the exothermic magnitude for both ΔH_f and ΔH_∞ of an alloy, simultaneously,

Please cite this article as: Keith A et al., Perspective of interstitial hydrides of high-entropy alloys for vehicular hydrogen storage, International Journal of Hydrogen Energy, https://doi.org/10.1016/j.ijhydene.2023.01.141

Table 1 – Alloys and intermetallic compounds investigated for hydrogen storage with date of publication, lattice type, alloy mass (g mol^{-1}), molar uptake (*H/M*) and gravimetric uptake (wt%). When the lattice type of the alloy shows X/Y this refers to a multi-phase materials with both X and Y lattices. X → Y refers to the phase transformation from alloy X into hydride Y. The sign '-' was inserted for data that has not been given in the relevant publication.

Alloys Synthesised	Publication Date	Lattice Structure	Alloy Mass (g mol^{-1})	*H/M*	wt%
TiVZrCrFeNi [30]	Mar-13	C14	59.17	1.00	1.56
TiVZrNbMo [31]	Mar-14	BCC	77.49	1.67	1.78
TiVZrNbHf [26]	Feb-16	BCC→BCT →FCC	92.29	2.50	2.70
TiZrNbHfTa [17]	Feb-19	BCC→BCT →FCC	118.29	2.00	1.68
TiZrNbHf [32]	Jun-19	BCC→FCC	101.90	2.00	1.94
TiVZrNb [32]	Jun-19	BCC→FCC	71.50	2.05	2.81
TiVNbHf [32]	Jun-19	BCC→FCC	92.56	1.95	2.08
TiVNbTa [32]	Jun-19	BCC→FCC	93.18	1.85	1.97
TiVCrNb [32]	Jun-19	BCC	60.94	1.90	3.05
TiVNbMo [32]	Jun-19	BCC	71.92	1.55	2.13
TiVCrNbTa [32]	Jun-19	BCC	84.94	1.80	2.10
TiVCrNbMo [32]	Jun-19	BCC	67.94	1.40	2.04
TiVCrMo [32]	Jun-19	BCC	61.70	0.75	1.21
$Ti_{0.325}V_{0.275}Zr_{0.125}Nb_{0.275}$ [33]	Jul-19	BCC→BCT	67.82	1.80	2.61
$TiV_{0.60}Cr_{0.30}Zr_{0.30}NbMo$ [34]	Sep-19	BCC/C14	73.88	0.90	1.20
$TiVZr_{0.15}NbTa_{0.85}$ [35]	Nov-19	BCC→FCC	89.59	1.85	2.02
$TiVZr_{0.50}NbTa_{0.50}$ [35]	Nov-19	BCC→FCC	81.78	1.89	2.26
$TiVZr_{0.74}NbTa_{0.26}$ [35]	Nov-19	BCC→FCC	76.13	1.95	2.50
TiVZrNb [35]	Nov-19	BCC→FCC	70.74	2.06	2.83
$TiVZr_{1.20}Nb$ [35]	Nov-19	BCC→FCC	71.56	1.99	2.71
$TiVZr_{1.50}Nb$ [35]	Nov-19	BCC→FCC	72.29	1.94	2.62
$TiVZr_{1.75}Nb$ [35]	Nov-19	BCC→FCC	74.02	1.80	2.37
$TiVZr_2Nb$ [35]	Nov-19	BCC→FCC	74.84	2.05	2.66
$Ti_{0.20}Zr_{0.20}Hf_{0.20}Nb_{0.40}$ [36]	Jan-20	BCC→FCC	100.69	1.14	1.12
$Ti_{0.20}Zr_{0.20}Hf_{0.20}Nb_{0.30}Mo_{0.10}$ [36]	Jan-20	BCC→FCC	100.99	1.58	1.54
$Ti_{0.20}Zr_{0.20}Hf_{0.20}Nb_{0.20}Mo_{0.20}$ [36]	Jan-20	BCC→FCC	101.29	1.21	1.18
$Ti_{0.20}Zr_{0.20}Hf_{0.20}Nb_{0.10}Mo_{0.30}$ [36]	Jan-20	BCC→BCT	101.60	1.44	1.40
$Ti_{0.20}Zr_{0.20}Hf_{0.20}Mo_{0.40}$ [36]	Jan-20	BCC→BCT	101.90	0.95	0.92
MgVTiCrFe [37]	Feb-20	BCC/Amorphous	46.20	0.35	0.15
TiZrNbTa [38]	Feb-20	BCC	102.69	1.05	1.25
TiCrMnFeNiZr [39]	Mar-20	C14	60.10	1.00	1.20
AlCrFeMnNiW [40]	Jul-20	BCC/FCC	72.05	0.41	0.61
$TiVZrNbHf_{0.5}$ [41]	Dec-20	BCC	82.71	2.00	2.38
$TiVZr_{0.5}NbHf$ [41]	Dec-20	BCC	92.41	1.99	2.13
$TiVZrNb_{0.5}Hf$ [41]	Dec-20	BCC	92.22	1.82	1.95
TiVZrHf [41]	Dec-20	BCC→ Degradation on hydrogenation	92.14	–	–
$TiV_{0.5}ZrNbHf$ [41]	Dec-20	BCC	96.89	1.96	2.00
$Ti_{0.5}ZrNbHf$ [41]	Dec-20	BCC	110.45	1.97	1.77
VZrNbHf [41]	Dec-20	BCC→ Degradation on hydrogenation	103.39	–	–
$Mg_{0.28}V_{0.28}Al_{0.19}Cr_{0.19}Ni_{0.6}$ [42]	Jan-21	BCC	39.60	0.15	0.30
$Mg_{0.10}Ti_{0.30}V_{0.25}Zr_{0.10}Nb_{0.25}$ [43]	Mar-21	BCC→FCC	83.86	1.50	2.40
MgAlTiFeNi [44]	Mar-21	BCC/FCC	42.75	0.07	0.94
$TiZrHfNb_2$ [45]	Mar-21	BCC→FCC	100.69	1.14	1.12
TiVCrZrNb [27]	Mar-21	FCC/BCC	66.99	1.21	1.77
$(TiVNb)_{0.65}Cr_{0.35}$ [46]	May-21	BCC	59.75	1.70	2.70
$(TiVNb)_{0.85}Cr_{0.15}$ [47]	Jun-21	BCC	62.13	1.79	3.18
$(TiVNb)_{0.95}Co_{0.05}$ [47]	Jun-21	BCC	63.68	1.76	2.77
$(TiVNb)_{0.962}Ni_{0.038}$ [47]	Jun-21	BCC	63.72	1.76	2.77
$Mg_{0.13}Al_{0.11}Ti_{0.33}Mn_{0.11}Nb_{0.33}$ [48]	Jun-21	BCC	58.64	1.00	1.70
TiZrNbCrFe [49]	Jul-21	C14/BCC → C14/FCC	67.98	1.32	1.90
$Ti_{0.20}Zr_{0.20}Nb_{0.20}V_{0.20}Cr_{0.17}Fe_{0.03}$ [50]	Sep-21	FCC/BCC	67.11	1.50	1.49
$Ti_{0.25}Zr_{0.25}Nb_{0.15}V_{0.15}Ta_{0.20}$ [51]	Dec-21	BCC	92.55	1.57	1.70
$(TiVFeZr)_{0.90}Al_{0.10}$ [52]	Feb-22	C14/HCP/BCT	58.03	0.75	1.30
TiZrCrNiMn [53]	Mar-22	C14	60.95	0.91	1.50

Please cite this article as: Keith A et al., Perspective of interstitial hydrides of high-entropy alloys for vehicular hydrogen storage, International Journal of Hydrogen Energy, https://doi.org/10.1016/j.ijhydene.2023.01.141

Table 2 – Hydrogen affinity of individual metal components (heats of formation model) [62]. 'N/A' refers to values that were have not been calculated. X* refers to an element which is somewhat intermediate in its affinity or lack thereof. It is neither strongly negative, nor positive in its values for ΔH_∞ or ΔH_f.

Element	Atomic no.	ΔH_∞ (kJ mol^{-1})	ΔH_f (kJ mol^{-1} H)	Type
Li	3	−51	−97	A
Be	4	−2	N/A	A*
Na	11	2	−56	A
Mg	12	27	−37	A
Al	13	63	3	B
Si	14	180	N/A	B
K	19	N/A	−58	A
Ca	20	N/A	−94	A
Sc	21	−90	−100	A
Ti	22	−52	−68	A
V	23	−30	−42	A
Cr	24	28	−6	B
Mn	25	1	−8	B*
Fe	26	30	10	B
Co	27	26	15	B
Ni	28	10	−3	B*
Cu	29	55	N/A	B
Zn	30	15	N/A	B*
Y	39	−79	−91	A
Zr	40	−52	−82	A
Nb	41	−38	−44	A
Mo	42	34	5	B
Ag	47	63	N/A	B
Sn	50	125	N/A	B
La	57	−67	−97	A
Hf	72	−38	−66	A
Ta	73	−36	−38	A
W	74	96	N/A	B

the higher the reported molar uptake (Fig. 2). Thus, the endothermic ΔH_∞ for the aforementioned alloys $Mg_{0.28}V_{0.28}Al_{0.19}Cr_{0.19}Ni_{0.06}$ and AlCrFeMnNiW can potentially explain the observed poor uptake.

To demonstrate the efficacy of the semi-empirical model by Griessen and Driessen for HEAs, Strozi et al. adapted the approach to account for multicomponent alloys [48]. In their approach, they do not only aim at predicting the likelihood of hydride formation based on the hydrogen affinity of an alloy, but also at its tailoring for the introduction of lightweight elements, in this instance Mg [48].

In order to better understand the utility of Mg-integration into HEAs and for hydrogen-storage applications in general, it is useful to consider the binary hydride of MgH_2. This compound has often been considered as a very promising candidate for solid-state hydrogen storage. This is due to the favourable gravimetric (7.6 wt%) and molar ($H/M = 2$) uptakes of hydrogen [9]. However, despite the ease of hydride formation ($\Delta H_f = -37$ kJ mol^{-1}) [48], the enthalpy of solution is a strongly endothermic process ($\Delta H_\infty = +21$ kJ mol^{-1}) [48]. In order to release the hydrogen from the MgH_2 lattice, elevated temperatures (350–400 °C) are necessary [64]. This thermal decomposition is impractical for large-scale use due to the high temperatures of operation, coupled with issues of poor thermal conductivity in the hydride, especially for vehicular applications.

In order to reduce the temperature of desorption from that of pure Mg, while retaining the beneficial mass reduction from not using 4*d* or 5*d* transition metals, such as Nb and Ta that are commonly used, Strozi et al., amongst others, have sought to incorporate Mg into HEAs. The HEA MgAlTiMnNb was computationally analysed by Strozi et al. in terms of four parameters (Table 4), in order to find the composition, which fulfils the following conditions.

- 'φ' parameter $\geq$20 (which predicts the likelihood of single-phase formation of the alloy – more details can be found in the section "*Elemental Distribution within Alloys*" below);
- valence electron concentration (*VEC*) > 6.87 (which has been proposed, as a working hypothesis, to predict temperatures of desorption [32], and the likelihood of forming a desired lattice, *i.e.* BCC or FCC - more details for this can be found in the section "*VEC*" below);
- the enthalpy of solution at infinite dilution ΔH_∞ is strongly exothermic;
- the enthalpy of formation of the concentrated hydride ΔH_f is also strongly exothermic [48].

As discussed above, the hydrogen affinity is dependent on the ΔH_∞ and ΔH_f values. What is especially noteworthy in this case, however, is the variation in affinity of the alloy with the manipulation of stoichiometric proportions. As stated

Please cite this article as: Keith A et al., Perspective of interstitial hydrides of high-entropy alloys for vehicular hydrogen storage, International Journal of Hydrogen Energy, https://doi.org/10.1016/j.ijhydene.2023.01.141

Table 3 – Hydrogen affinity values (calculated using equation (1) &2) and hydrogen uptake of the given alloys. For values containing one metal element, or more, where either ΔH_∞ and or ΔH_f were denoted as N/A, these values were taken to be equal to zero. This is, however, not an accurate approximation, and could lead to inaccurate qualitative values for the affinity values of said alloys.

Alloys Synthesised	ΔH_∞ (kJ mol^{-1})	ΔH_f (kJ mol^{-1})	H/M	wt%
AlCrFeMnNiW	38.00	−0.67	0.41	0.61
HfNbTiVZr	−42.00	−60.40	2.50	2.70
MgAlTiFeNi	15.60	−19.00	0.07	0.94
$Mg_{0.13}Al_{0.11}Ti_{0.33}Mn_{0.11}Nb_{0.33}$	−19.15	−42.32	1.00	1.70
$Mg_{0.28}V_{0.28}Al_{0.19}Cr_{0.19}Ni_{0.6}$	17.05	−22.87	0.15	0.30
MgVTiCrFe	0.60	−28.60	0.35	0.15
$MgZrTiFe_{0.50}Co_{0.50}Ni_{0.50}$	−5.78	−37.78	0.70	1.20
$TiV_{0.6}Cr_{0.3}Zr_{0.3}NbMo$	−19.33	−37.76	0.90	1.20
$(TiVNb)_{0.65}Cr_{0.35}$	−16.20	−35.47	1.70	2.70
$Ti_{0.30}V_{0.25}Zr_{0.10}Nb_{0.25}Mg_{0.10}$	−10.70	−87.00	1.50	2.40
TiZrCrMnFeNi	−5.83	−26.17	1.00	1.20
$TiZrHfNb_2$	−43.60	−60.80	1.03	1.02
TiZrNbCrFe	−16.80	−38.00	1.32	1.90
TiZrNbHfTa	−43.20	−59.60	2.00	2.09
TiZrNbMoV	−31.51	−50.37	1.67	1.78
TiZrNbTa	−44.73	−58.86	1.05	1.25
TiZrNbVCr	−28.80	−48.40	1.21	1.77
ZrTiVCrFeNi	−13.44	−33.42	1.00	1.56
$Ti_{0.20}Zr_{0.20}Nb_{0.20}V_{0.20}Cr_{0.17}Fe_{0.03}$	−28.74	−47.92	1.50	1.49
$Ti_{0.25}Zr_{0.25}Nb_{0.15}V_{0.15}Ta_{0.20}$	−43.40	−58.00	1.57	1.70
TiZrCrNiMn	−13.00	−33.40	0.91	1.50
$(ZrTiFeV)_{0.90}Al_{0.10}$	−17.10	−40.65	0.75	1.30
$Ti_{0.325}V_{0.275}Zr_{0.125}Nb_{0.275}$	−43.50	−57.84	1.80	1.70
$(TiVNb)_{0.85}Cr_{0.15}$	−29.80	−44.53	1.79	3.18
$(TiVNb)_{0.953}Co_{0.047}$	−36.90	−48.22	1.76	2.77
$(TiVNb)_{0.962}Ni_{0.038}$	−38.10	−49.50	1.76	2.77
$TiVZr_{0.15}NbTa_{0.85}$	−39.64	−49.76	1.85	2.02
$TiVZr_{0.50}NbTa_{0.50}$	−40.90	−53.34	1.89	2.26
$TiVZr_{0.74}NbTa_{0.26}$	−42.04	−56.36	1.95	2.50
TiVZrNb	−43.00	−59.00	2.06	2.83
$TiVZr_{1.20}Nb$	−43.36	−59.92	1.99	2.71
$TiVZr_{1.50}Nb$	−43.56	−60.94	1.94	2.62
$TiVZr_{1.75}Nb$	−44.44	−62.68	1.80	2.37
$TiVZr_2Nb$	−44.80	−63.60	2.05	2.66
$Ti_{0.20}Zr_{0.20}Hf_{0.20}Nb_{0.40}$	−43.60	−60.80	1.14	1.12
$Ti_{0.20}Zr_{0.20}Hf_{0.20}Nb_{0.30}Mo_{0.10}$	−36.40	−55.90	1.58	1.54
$Ti_{0.20}Zr_{0.20}Hf_{0.20}Nb_{0.20}Mo_{0.20}$	−29.20	−51.00	1.21	1.18
$Ti_{0.20}Zr_{0.20}Hf_{0.20}Nb_{0.10}Mo_{0.30}$	−22.00	−46.10	1.44	1.40
$Ti_{0.20}Zr_{0.20}Hf_{0.20}Mo_{0.40}$	−14.80	−41.20	0.95	0.92
TiZrNbHf	−14.80	−41.20	2.00	1.94
TiVZrNbHf	−27.60	−50.60	1.85	1.97
TiVZrNb	−25.00	−46.75	2.05	2.81
TiVNbHf	−39.50	−55.00	1.95	2.08
TiVNbTa	−39.00	−48.00	1.85	1.97
TiVCrNb	−23.00	−40.00	1.90	3.05
TiVNbMo	−21.50	−37.25	1.55	2.13
TiVCrNbTa	−25.60	−39.60	1.80	2.10
TiVCrNbMo	−11.60	−31.00	1.40	2.04
TiVCrMo	−5.00	−27.75	0.75	1.21
$TiVZrNbHf_{0.50}$	−42.44	−59.78	2.00	2.38
$TiVZr_{0.50}NbHf$	−40.89	−58.00	1.99	2.13
$TiVZrNb_{0.50}Hf$	−42.44	−62.22	1.82	1.95
$TiV_{0.50}ZrNbHf$	−43.33	−62.44	1.96	2.00
$Ti_{0.50}ZrNbHf$	−44.00	−64.57	1.97	1.77

Please cite this article as: Keith A et al., Perspective of interstitial hydrides of high-entropy alloys for vehicular hydrogen storage, International Journal of Hydrogen Energy, https://doi.org/10.1016/j.ijhydene.2023.01.141

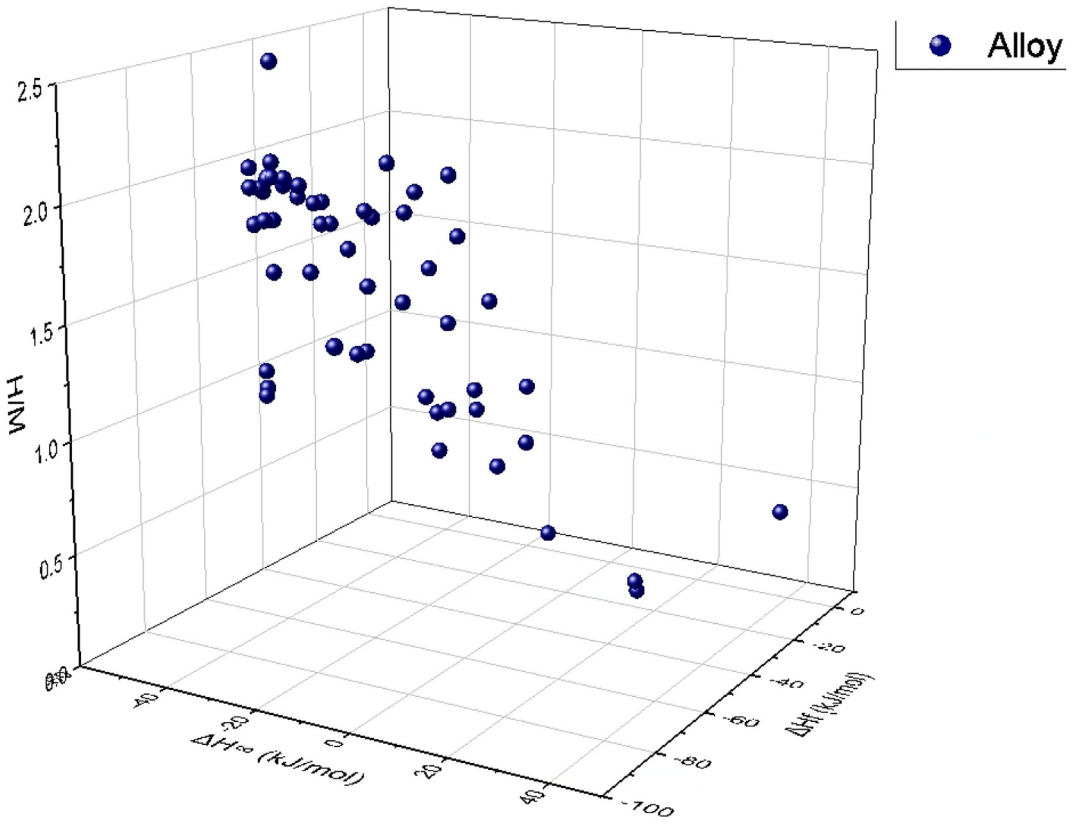

Fig. 2 – Enthalpy of solution at infinite dilution and enthalpy of hydride formation shown relative to the molar uptake of hydrogen for a given alloy.

Table 4 – Summary of the calculations conducted by Strozi et al. for the equiatomic and the optimised alloys MgAlTiMnNb and $Mg_{12}Al_{11}Ti_{33}Mn_{11}Nb_{33}$, with the comparison drawn between them, $Mg_{0.28}V_{0.28}Al_{0.19}Cr_{0.19}Ni_{0.6}$ and Mg as a pure metal.

Parameter/Alloy	MgAlTiMnNb	$Mg_{0.12}Al_{0.11}Ti_{0.33}Mn_{0.11}Nb_{0.33}$	$Mg_{0.28}V_{0.28}Al_{0.19}Cr_{0.19}Ni_{0.6}$	Mg
φ	12.1	20.7	N/A	N/A
ΔH_f (kJ mol^{-1})	−32.2	−42.7	−22.9	−37.0
ΔH_∞ (kJ mol^{-1})	−8.0	−24.0	17.1	+21.0
VEC	4.20	4.31	4.21	2.00
H/M	N/A	1.00	0.15	2.00

previously, Mg has an unfavourable, endothermic value for ΔH_∞ (+21 kJ mol^{-1}) [48], and this makes the dissolution of hydrogen through the lattice unfavourable. By forming an HEA containing Mg and transition metals that have a strongly exothermic ΔH_∞ value, such as Nb and Ti with respective ΔH_∞ values of −38 kJ mol^{-1} and -52 kJ mol^{-1}, the hydrogen uptake increases.

Comparing the theoretical, equimolar MgAlTiMnNb with the optimised $Mg_{0.12}Al_{0.11}Ti_{0.33}Mn_{0.11}Nb_{0.33}$ alloy, reducing the stoichiometric proportion of Mg, Mn, and Al – the latter two of which have ΔH_∞, and ΔH_f values of ΔH_∞ = 1 kJ mol^{-1}, and 63 kJ mol^{-1}; ΔH_f = −8 kJ mol^{-1} and 3 kJ mol^{-1} respectively [62] – and increasing that of Ti and Nb offers an increase in the overall affinity from −32.2 to −42.7 kJ mol^{-1}for ΔH_f and −8.0 kJ mol^{-1} to −24.0 kJ mol^{-1} for ΔH_∞. When comparing the optimised $Mg_{0.12}Al_{0.11}Ti_{0.33}Mn_{0.11}Nb_{0.33}$ further with another HEA previously formed by Strozi et al. that also incorporated Mg, $Mg_{0.28}V_{0.28}Al_{0.19}Cr_{0.19}Ni_{0.6}$, the molar uptake of the alloy is very low at *H/M* = 0.15 – despite an exothermic value for ΔH_f [48]. This can potentially be explained by the endothermic value for ΔH_∞ for $Mg_{0.28}V_{0.28}Al_{0.19}Cr_{0.19}Ni_{0.6}$ (ΔH_∞ = 17.1 kJ mol^{-1}) hindering the dissolution of hydrogen throughout the lattice.

Tailoring the affinity values of an alloy is therefore very useful as the benefits of incorporating lightweight elements such as Al or Mg are retained, *i.e.* a decrease in the molar mass improving gravimetric capacity, while offering a reduction in the desorption temperature; *e.g.* the onset desorption temperature for MgH_2 is 330 °C [64] and 275 °C for $Mg_{12}Al_{11}Ti_{33}Mn_{11}Nb_{33}$ [48].

While the gravimetric capacity of 1.70% for $Mg_{12}Al_{11}Ti_{33}Mn_{11}Nb_{33}$ is relatively high in relation to previously investigated HEAs, the molar uptake remains low as 1.0 [48]. This may be in part due to the nature of the bonding between the metal (Mg *v* Nb and Ti) as, in particular, the bond is more ionic in character for MgH_2 [65], in comparison to the bonding

Please cite this article as: Keith A et al., Perspective of interstitial hydrides of high-entropy alloys for vehicular hydrogen storage, International Journal of Hydrogen Energy, https://doi.org/10.1016/j.ijhydene.2023.01.141

observed in interstitial hydrides [66]. This could potentially lead to a destabilisation of the hydrogen in the interstices, as in the case of Mg the dilution of hydrogen amongst the lattice is not favourable (indicated by ΔH_{∞}).

Therefore, instead of forming alloys with Mg, utilising lightweight transition metals that afford more metallic bonding with hydrogen, such as V, could prove a remedy to the difference in bonding without drastically increasing the mass of the alloy and likewise maintaining the advantageous hydrogen affinity.

Alongside hydrogen affinity, other parameters are just as important in order to promote the highest possible hydrogen capacity in prospective HEAs. By analysing these alloys, with particular attention paid to their most fundamental properties and behaviours, it is possible to further understand the driving forces behind elevated hydrogen storage in these alloys. One such parameter is the valence electron concentration and its effects.

Valence electron concentration

A key parameter that is intrinsic to every metal, elemental or alloyed, and its consequent properties/behaviours, is the Valence Electron Concentration (*VEC*). The *VEC* of an element (Table 5) is the total number of electrons located within the valence band – for transition metals, this includes the highest order *s*- and *d*-electrons *i.e.* for Ti ([Ar] $4s^2$ $3d^2$) the *VEC* is four [67] – with the *VEC* of an alloy being the weighted average of the *VEC*s of the elements present in the HEA, based on their stoichiometric contribution to the final alloy (Equation (3)), and can potentially be used to predict various properties.

Table 5 – *VEC* of various metal elements.

Element	Atomic no.	VEC [69]
Li	3	1
Na	11	1
Mg	12	2
Al	13	3
K	19	1
Ca	20	2
Sc	21	3
Ti	22	4
V	23	5
Cr	24	6
Mn	25	7
Fe	26	8
Co	27	9
Ni	28	10
Cu	29	11
Zn	30	12
Y	39	3
Zr	40	4
Nb	41	5
Mo	42	6
La	57	3
Hf	72	4
Ta	73	5
W	74	6

Most pertinently to the current discussion, as outlined by Guo et al. [68], the parameter can be used to enable and/or explain the formation of certain crystal packing arrangements of the resultant alloy. FCC lattices are more energetically favourable at higher *VEC* (>8), and BCC at a lower *VEC* (<6.87) [68]. Within the range of 6.87–8.00, there is bi-phasal behaviour, *i.e.* the formation of both BCC and FCC is observed [40].

Moreover, this is not the only domain where the *VEC* of an alloy could be used to tailor properties. It could potentially be used to estimate the temperature of hydrogen desorption from the hydride. While investigating the possible effects relating to hydrogen sorption in various TiVNb-based HEAs, Nygård et al. observed a linear relationship between the onset temperature of the first hydrogen-desorption event off the alloy (T_{onset}) and the *VEC* from experimental data (Equation (4)) [32]. This relationship suggests that for higher *VEC* the T_{onset} is lowered. With the aim to ultimately achieve the US DOE's targets for reversible storage (between −40 °C and 60 °C at 5–12 bar), the *VEC* of the alloy appears to be a useful empirical parameter. It must be stressed that however, to the best of the authors' knowledge at the time of writing, this is a working hypothesis, with neither corroboration nor contradiction found in any publications.

In the case of this hypothesis being validated, from the relationship derived by Nygård et al., having a *VEC* in the region between 6.32 and 6.86, would result in a desorption temperature in line with the US Department of Energy's aims of near-room-temperature conditions, which is estimated to be achieved when the *VEC* is 6.40 [6]. From the perspective of lattice formation, as we know that for the *VEC* ≤ 6.87 a BCC lattice is predicted to be the most likely to form, which contains the ideal range for US DOE targets for thermodynamics of ad-/desorption.

$$VEC = \sum_{i=1}^{N} c_i VEC_i \tag{3}$$

Equation (3): Formula for evaluating the *VEC* of a given alloy. c_i = stoichiometry of element *i*; VEC_i = *VEC* of metal element *i* when pure [32].

$$T_{onset} = 1,203\ ^{\circ}C - (VEC \times 184^{\circ}C) \tag{4}$$

Equation (4): Formula describing the temperature of the first hydrogen desorption event of a given alloy. T_{onset} = onset temperature of the first desorption event; *VEC* = valence electron count of the given HEA [32].

In addition, the TiVNb-based alloys investigated by Nygård et al. – that were used to propose the relationship for the T_{onset} given above – initially formed BCC alloys that distort into FCC hydrides upon hydrogenation [32]. This distortion occurred only in certain circumstances and varies with the increase in *VEC* [32].

Upon hydrogenation, when.

- the initial BCC alloy has a *VEC* < 4.75, a single-phase FCC hydride was obtained.
- the initial BCC alloy has a *VEC* has a value between 4.75 and 5.00 FCC hydride were formed.
- the initial BCC alloy has a *VEC* > 5.00, this FCC hydride phase did not form, and the hydride retained the initial BCC structure [32].

Please cite this article as: Keith A et al., Perspective of interstitial hydrides of high-entropy alloys for vehicular hydrogen storage, International Journal of Hydrogen Energy, https://doi.org/10.1016/j.ijhydene.2023.01.141

The alloys that report the highest molar uptakes of hydrogen follow a BCC → (*pseudo*-)FCC distortion upon hydrogenation (TiVZrNbHf [26], TiNbZrHfTa [17], and $TiVZr_2Nb$ [32] to name but a few) for which maintaining a *VEC* < 4.75 would be advisable.

To summarise, the preferential formation of BCC alloys can be engineered by adjusting the *VEC*, and the BCC structure can preferentially distort into a (*pseudo*-)FCC lattice when the hydride forms. The temperature of desorption might also be predicted from the *VEC* value. However, a key concern when synthesising HEAs is the formation of multiple phases during the synthesis of the alloy. Therefore, how can this be avoided?

Elemental distribution within alloys

In order for an alloy to have a reliable performance, it is advantageous for the structure to be "homogenous". Homogeneity can be defined in two ways: the lattice is homogenous *i.e.* a single-phase lattice type *e.g.* BCC/FCC *etc.*, and the distribution of the elements is random throughout the lattice. Ensuring the randomised distribution of elements avoids phase separation in the alloy, as the elements that have a high affinity for one another will not form separate intermetallic phases and instead form the preferred solid solution.

Therefore, to maximise the benefits of the formation of a BCC, ensuring the randomised distribution of the elements throughout the lattice is required. Multi-phase alloys (Table 6) are common when it comes to hydrogen absorbing materials. Therefore, the formation of a single-phase structure for the alloy, prior to hydride formation, is advantageous for obtaining the highest hydrogen capacity.

Ideally, single-phase HEAs are obtained by design, in line with a hard-spheres model purported by Mansooris [70]. Ye et al. proposed a possible method by which to ascertain the likelihood of single-phase formation, using the φ parameter (Equations (5)–(9)) [71].

$$\varphi = \frac{S_c \frac{\Delta H_{mix}}{T_m}}{|S_E|} \tag{5}$$

$$\Delta H_{Mix} = \sum_{i=1;i\neq j}^{n} 4\Delta H_{ij}^{Mix} c_i c_j \tag{6}$$

$$T_m = \sum_{i=1}^{n} c_i (T_m)_i \tag{7}$$

$$S_c = -k_B \sum_{j=1}^{n} c_i \, ln \, c_i \tag{8}$$

$$|S_E| = -\frac{\left(\frac{(F-F_{id})}{Nk_BT} - \ln(Z)\right)}{Nk_B} \tag{9}$$

Equation (5): Relationships used to find φ. Equation (6): Equation to derive the enthalpy of mixing of the elements present in the alloy, ΔH_{mix}, where $\Delta H_{mix(ij)}$ is the enthalpy of mixing of elements *i* and *j*, c_i is the stoichiometric proportion of element *i* in the resultant alloy, and c_j is the stoichiometric proportion of element *j* in the resultant alloy [72]. Equation (7): The average melting temperature of the elements found in the alloy, T_m, c_i is the stoichiometric proportion of element *i* in the

Table 6 – BCC-phase containing HEAs previously investigated for their hydrogen storage capabilities. X→Y refers to the lattice of the metal distorting from the alloy X into hydride with structure Y upon hydrogenation. X→A→Y refers to the distortion of alloy X into hydride Y *via* a partially hydrogenated intermediate structure A.

Alloy	Structure
AlCrFeMnNiW	BCC/FCC
HfNbTiVZr	BCC→BCT→FCC
MgAlTiFeNi	BCC/FCC
$Mg_{0.13}Al_{0.11}Ti_{0.33}Mn_{0.11}Nb_{0.33}$	BCC
$Mg_{0.28}V_{0.28}Al_{0.19}Cr_{0.19}Ni_{0.6}$	BCC
MgVTiCrFe	BCC/Amorphous
$MgZrTiFe_{0.5}Co_{0.5}Ni_{0.5}$	BCC→FCC
$TiV_{0.6}Cr_{0.3}Zr_{0.3}NbMo$	BCC/C14
$(TiVNb)_{0.65}Cr_{35}$	BCC
$Ti_{0.30}V_{0.25}Zr_{0.10}Nb_{0.25}Mg_{0.10}$	BCC→FCC
$TiZrHfNb_2$	BCC→FCC
TiZrNbCrFe	C14/BCC → C14/FCC
TiZrNbHfTa	BCC→BCT→FCC
TiZrNbMoV	BCC
TiZrNbVCr	FCC/BCC
ZrTiVCrFeNi	C14
$Ti_{0.20}Zr_{0.20}Nb_{0.20}V_{0.20}Cr_{0.17}Fe_{0.03}$	FCC/BCC
$Ti_{0.25}Zr_{0.25}Nb_{0.15}V_{0.15}Ta_{0.20}$	BCC
$Ti_{0.325}V_{0.275}Zr_{0.125}Nb_{0.275}$	BCC→BCT
$(TiVNb)_{0.85}Cr_{0.15}$	BCC
$(TiVNb)_{0.953}Cr_{0.047}$	BCC
$(TiVNb)_{0.962}Cr_{0.038}$	BCC
$TiVZr_{0.15}NbTa_{0.85}$	BCC→FCC
$TiVZr_{0.50}NbTa_{0.50}$	BCC→FCC
$TiVZr_{0.74}NbTa_{0.26}$	BCC→FCC
TiVZrNb	BCC→FCC
$TiVZr_{1.20}Nb$	BCC→FCC
$TiVZr_{1.50}Nb$	BCC→FCC
$TiVZr_{1.75}Nb$	BCC→FCC
$TiVZr_2Nb$	BCC→FCC
$Ti_{0.20}Zr_{0.20}Hf_{0.20}Nb_{0.40}$	BCC→FCC
$Ti_{0.20}Zr_{0.20}Hf_{0.20}Nb_{0.30}Mo_{0.10}$	BCC→FCC
$Ti_{0.20}Zr_{0.20}Hf_{0.20}Nb_{0.20}Mo_{0.20}$	BCC→FCC
$Ti_{0.20}Zr_{0.20}Hf_{0.20}Nb_{0.10}Mo_{0.30}$	BCC→BCT
$Ti_{0.20}Zr_{0.20}Hf_{0.20}Mo_{0.40}$	BCC→BCT
TiZrNbHf	BCC→FCC
TiVZrNbHf	BCC→FCC
TiVZrNb	BCC→FCC
TiVNbHf	BCC→FCC
TiVNbTa	BCC→FCC
TiVCrNb	BCC
TiVNbMo	BCC
TiVCrNbTa	BCC
TiVCrNbMo	BCC
TiVCrMo	BCC
$TiVZrNbHf_{0.50}$	BCC
$TiVZr_{0.50}NbHf$	BCC
$TiVZrNb_{0.50}Hf$	BCC
TiVZrHf	BCC
$TiV_{0.50}ZrNbHf$	BCC
$Ti_{0.50}ZrNbHf$	BCC
VZrNbHf	BCC

Please cite this article as: Keith A et al., Perspective of interstitial hydrides of high-entropy alloys for vehicular hydrogen storage, International Journal of Hydrogen Energy, https://doi.org/10.1016/j.ijhydene.2023.01.141

resultant alloy, and $T_{m(i)}$ is the melting temperature of element i when pure [72]. Equation (8): The relationship describing the entropy of conformation S_c where k_B is the Boltzmann constant, and c_i is the stoichiometry of element i in the alloy. Equation (9): The equation to derive the excess entropy of mixing, S_E (See Supplementary Information for more details) [70].

S_c is the configurational entropy for an ideal gas (Equation (8)) – where k_B is Boltzmann's constant, and c_i is the molar fraction of the ith element [73] – S_E is the excess entropy of mixing that is a function of atomic packing and atom size (0.68 for BCC, 0.74 for FCC lattices [72]) (Equation (7)), T_m the average melting temperature, and ΔH_{mix} the enthalpy of mixing (a more detailed view of the calculations required to determine φ can be found in the Supplementary Information).

The results from the calculations show that.

- For $\varphi < 10$, multiphase (amorphous) behaviour is observed.
- For $11 < \varphi < 20$, a mixture of both single and amorphous phases are reported.
- For $\varphi > 20$, single phase behaviour is observed [71].

As discussed previously, Strozi et al. have adapted this approach to the formation of HEAs with the random distribution of elements [48]. Despite the utility of this robust approach, the calculations can be lengthy, especially when used *ab initio* in order to assess the random elemental distribution of many prospective structures, in the same way as Strozi et al.; as the number of iterations required for a complete analysis increases, the more time-consuming the process becomes.

In contrast, Yang et al. offer a bi-dimensional approach utilising more concise calculations for typical multicomponent HEAs by calculating parameters of crystal packing distortion [72]: δ (Equation (10)) and the Ω parameter (Equation (11)). Where δ is a measure of the variation of size of the constituent metals, and the Ω parameter is essentially a thermodynamic parameter, which gives some insight into the stability of the resultant solution [72]. Ω is, ostensibly, a measurement of the free energy of mixing for the components in its proposed composition (ΔG_{mix}) and fluctuates with respect to the enthalpy and entropy of mixing (ΔH_{mix} and ΔS_{mix}) of the given conformation.

$$\delta = \sqrt{\sum_{i=1}^{N} c_i \left(1 - \frac{r_i}{\bar{r}}\right)^2} \tag{10}$$

$$\Omega = \frac{\Delta S_{mix} T_m}{|\Delta H_{Mix}|} \tag{11}$$

$$\Delta S_{Mix} = -R \sum_{i=1}^{n} c_i \ln c_i \tag{12}$$

Equation (10): Formula describing the δ of a given alloy. $c_{i\text{-}}$ = stoichiometry of component c; r_i = radius of metal component when pure; $\bar{r}$ = mean radius of the elements present in the alloy [72]. Equation (11): The relationship used to for calculate the Ω value of an alloy where ΔH_{mix} and T_m are calculated using Equations (5) and (6) (see above), and ΔS_{mix} is calculated using Equation (11) [72]. Equation (12): The entropy of mixing where R is the ideal gas constant, and c_i is the stoichiometry of element i in the alloy [72].

ΔH_{mix} is calculated using Miedma's model in relation to HEAs for hydrogen sorption [26,27,30,40,42,72]; the larger the magnitude of the ΔH_{mix}, positive or negative, the more the random distribution of the elements, and hence the formation of a solid solution, is resisted [72]. For strongly exothermic ΔH_{mix}, *e.g.* for Nb + Ni ΔH_{mix} −30 kJ mol^{-1}, the formation of NbNi phases is thermodynamically more favourable than the solid solution, thus the random distribution of elements is not achieved and phase separation occurs [72]. The reverse is also true, where elements that have a strongly endothermic ΔH_{mix}, *e.g.* Zn and W where ΔH_{mix} = 15 kJ mol^{-1}, the mixing of these elements does not allow random distribution as the miscibility of the elements is reduced [72]. The entropic contribution is also noteworthy, as a solid solution forms when the distribution of the atoms is randomised. In other words, when the disorder in distribution of all elements throughout the lattice is high, a solid solution is preferentially formed [72]. Therefore, the value for ΔS_{mix} should be as large as possible to facilitate solid-solution formation for HEAs. This entropic effect is compounded when T_m is high as the variation in entropy is heavily affected by this temperature increase [72].

The authors, citing extensive *a posteriori* calculations of upwards of 60 alloys of the δ value and the Ω values of various multicomponent alloys, draw a comparison between the reported nature of the alloys – as intermetallic compounds, solid solutions, a combination of both, or bulk metallic glasses (*i.e.* amorphous), and their respective δ and Ω values [72]. They, therefore, concluded that solid-solution formation usually occurs between the values of $\delta \leq 6.6\%$ and $\Omega \geq 1.1$ [72]. For the previously synthesised alloys (Table 7), this suggests that the majority of HEAs assessed for hydrogen storage were within the regions of δ and Ω to be considered high-entropy alloys, with some outliers.

Considering and utilising the above parameters in the design of prospective HEA hydrogen carriers, we summarise that a good HEA contender.

1. Forms the most advantageous lattice structure, BCC, by tailoring the *VEC*, not going above 4.75, in order to ensure that the lattice distorts into a (*pseudo*-)FCC hydride upon hydrogenation.
2. Has a randomised distribution of the elements by obtaining $\Omega \geq 1.1$ and $\delta \leq 6.6$ or $\varphi \geq 20$.
3. Favourably forms a stable hydride by assessing and incorporating elements with advantageous values for both ΔH_{∞} and ΔH_f.
4. Lightweight elements can be incorporated into and avoid their unfavourable thermodynamics of desorption *e.g.* Mg.

Through adherence to the above criteria, the design of the interstitial hydride of an HEA with a high volumetric uptake of hydrogen can be obtained. These hydrides offer an increased volumetric and gravimetric capacity for hydrogen relative to traditional interstitial hydrides and may offer an increase relative to physical hydrogen-storage techniques. However, how can these considerations be realistically implemented?

Please cite this article as: Keith A et al., Perspective of interstitial hydrides of high-entropy alloys for vehicular hydrogen storage, International Journal of Hydrogen Energy, https://doi.org/10.1016/j.ijhydene.2023.01.141

Table 7 – Values for δ and Ω of all *HEAs* investigated for hydrogen uptake.

Alloy	Ω	δ%
AlCrFeMnNiW	11.07	9.80
HfNbTiVZr	38.38	4.55
MgAlTiFeNi	1.38	5.53
$Mg_{0.12}Al_{0.11}Ti_{0.33}Mn_{0.11}Nb_{0.33}$	360.78	4.98
$Mg_{0.28}V_{0.28}Al_{0.19}Cr_{0.19}Ni_{0.6}$	8.18	7.06
MgVTiCrFe	3.71	9.87
$MgZrTiFe_{0.5}Co_{0.5}Ni_{0.5}$	2.30	9.89
$TiV_{0.6}Cr_{0.3}Zr_{0.3}NbMo$	8.28	10.69
$(TiVNb)_{0.65}Cr_{0.35}$	7.31	5.95
$Ti_{0.30}V_{0.25}Zr_{0.1}Nb_{0.25}Mg_{0.1}$	3.59	6.57
TiZrCrMnFeNi	1.37	6.63
$TiZrHfNb_2$	8.33	9.88
TiZrNbCrFe	2.76	5.46
TiZrNbHfTa	12.37	9.79
TiZrNbMoV	11.67	6.84
TiZrNbTa	11.60	4.96
TiZrNbVCr	6.40	8.66
ZrTiVCrFeNi	1.66	10.02
$Ti_{0.2}Zr_{0.2}Nb_{0.2}V_{0.2}Cr_{0.17}Fe_{0.03}$	5.61	8.80
$Ti_{0.25}Zr_{0.25}Nb_{0.15}V_{0.15}Ta_{0.2}$	6.38	6.30
TiZrCrNiMn	1.13	13.06
$(ZrTiFeV)_{0.90}Al_{0.10}$	1.81	9.82
$Ti_{0.325}V_{0.275}Zr_{0.125}Nb_{0.275}$	82.28	9.36
$(TiVNb)_{0.85}Cr_{0.15}$	8.38	7.69
$(TiVNb)_{0.953}Co_{0.047}$	5.00	5.75
$(TiVNb)_{0.962}Ni_{0.038}$	3.78	4.93
$TiVZr_{0.15}NbTa_{0.85}$	105.13	3.93
$TiVZr_{0.50}NbTa_{0.50}$	45.28	4.69
$TiVZr_{0.74}NbTa_{0.26}$	28.52	5.94
TiVZrNb	20.69	6.54
$TiVZr_{1.20}Nb$	19.50	7.04
$TiVZr_{1.50}Nb$	18.35	7.18
$TiVZr_{1.75}Nb$	17.64	7.30
$TiVZr_2Nb$	15.36	7.36
$Ti_{0.20}Zr_{0.20}Hf_{0.20}Nb_{0.40}$	27.78	7.38
$Ti_{0.20}Zr_{0.20}Hf_{0.20}Nb_{0.30}Mo_{0.10}$	39.21	6.35
$Ti_{0.20}Zr_{0.20}Hf_{0.20}Nb_{0.20}Mo_{0.0}$	15.68	6.61
$Ti_{0.20}Zr_{0.20}Hf_{0.20}Nb_{0.10}Mo_{0.30}$	11.03	6.84
$Ti_{0.20}Zr_{0.20}Hf_{0.20}Mo_{0.40}$	8.54	7.04
TiZrNbHf	10.72	4.86
TiVZrNbHf	191.92	7.06
TiVNbHf	107.75	6.44
TiVNbTa	116.62	4.93
TiVCrNb	6.09	6.27
TiVNbMo	9.40	4.07
TiVCrNbTa	8.54	9.12
TiVCrNbMo	8.34	5.61
TiVCrMo	7.01	5.74
$TiVZrNbHf_{0.5}$	32171.7	7.10
$TiVZr_{0.5}NbHf$	163.81	6.88
$TiVZrNb_{0.5}Hf$	46.08	7.32
TiVZrHf	12.58	7.61

Perspective

It is worthwhile speculating how the aforementioned parameters can be adapted to the future study of these alloys. As stated previously, if the *VEC* of an alloy may predict the temperature of desorption of hydrogen, a range of 6.32–6.86 is required for DOE standards [6], however A type metals have a *VEC* range of ≤5. This could potentially explain why some HEAs have high T_{onset} values (Fig. 3).

To counteract this, potentially utilising high-*VEC* metals which do not compromise the affinity values is important. The metals with the most potential in this regard are Mn, Ni, and Zn (Table 8), with *VEC*s 7, 10, and 12 respectively, with ΔH_∞ and ΔH_f values that do not substantially compromise the overall affinity, as is the case with *e.g.* Co, Fe, or Al, nor do they significantly raise the mass of the resultant alloy, with molar masses of 54.94 g mol^{-1}, 58.70 g mol^{-1}, and 65.38 g mol^{-1} respectively – common metals implemented in these alloys, Nb and Zr have molar masses of 92.91 g mol^{-1} and 91.22 g mol^{-1} respectively [74].

For example, the alloy TiVZrNbCr has been previously synthesised and assessed for hydrogen uptake, with a reasonable hydrogen affinity. When instead of Cr (*VEC* = 6, $\Delta H_\infty = +28$ kJ mol^{-1}, $\Delta H_f = +6$ kJ mol^{-1}), Mn (*VEC* = 7, $\Delta H_\infty = +1$ kJ mol^{-1}, $\Delta H_f = -8$ kJ mol^{-1}), or Ni (*VEC* = 10, $\Delta H_\infty = +10$ kJ mol^{-1}, $\Delta H_f = -3$ kJ mol^{-1}), or Zn (*VEC* = 12, $\Delta H_\infty = +15$ kJ mol^{-1}, ΔH_f taken as = 0 kJ mol^{-1}, as the Griessen and Driessen Model does not give a specific value [62]) are used (Table 9), the affinity parameters values only slightly vary. However, the *VEC* shows an increase from 4.80 to 5.00, 5.60, and 6.00 for the Mn, Zn and Ni alloys respectively. This approach could increase the *VEC* towards the range for that would allow – in the case of corroboration of the findings released by Nygård et al. – the desorption temperatures (*VEC* = 6.32–6.86 [32]) outlined by the US Department of Energy [6]. In fact, the utilisation of Zn instead of Cr in this specific alloy brings δ to within the threshold set by Yang et al., an improvement on the Cr, Mn, and Ni alloys [72].

This does, however, ensure that the formation of the (*pseudo*-)FCC hydride does not occur [32], as the threshold for FCC hydride formation from a BCC alloy is *VEC* < 4.75 as outlined by Nygård et al., which may result in a reduced hydrogen capacity [32]. Therefore, to offer a higher capacity, implementing metals such as Sc or Y would keep the *VEC* below 4.75. This comes with the added benefit of a hydride with a substantially higher affinity, due to a greater proportion of A type metals being used. Varying the stoichiometry of the elements in the alloy may also prove useful in maintaining a balance between the *VEC*, the hydrogen affinity, and the homogeneity parameters.

For an FCC lattice, there are 12 interstitial sites that can be occupied, 8 tetrahedral, and 4 octahedral [75]. With 4 metal spheres per unit cell [75], the maximum molar uptake of hydrogen in this lattice type is 3 [75]. Scandium hydride has a high *H/M* = 2, which comes as little surprise given the impressive affinity values that Sc boasts ($\Delta H_\infty = -90$ kJ mol^{-1}; $\Delta H_f = -100$ kJ mol^{-1} [62]) and forms an FCC hydride. This would suggest that, as the tetrahedral sites are degenerate, all of these sites are occupied, with the octahedral sites unoccupied - and this holds true for *3d* transition metal hydrides with a molar uptake of 2. This results in a gravimetric uptake of 4.30 wt% for ScH_2, 4.05 wt% for TiH_2 and 3.81 wt% for VH_2. Forming an HEA hydride with an FCC lattice with *H/M* = 3 would require occupation of all of the tetrahedral and octahedral sites simultaneously. Were the alloy to be formed of lightweight elements, this could promote a very promising

Please cite this article as: Keith A et al., Perspective of interstitial hydrides of high-entropy alloys for vehicular hydrogen storage, International Journal of Hydrogen Energy, https://doi.org/10.1016/j.ijhydene.2023.01.141

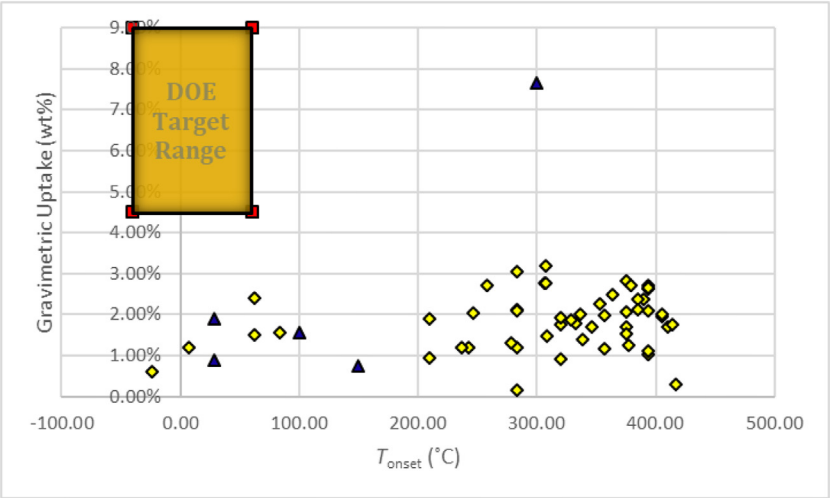

Fig. 3 – Figure illustrating the values for the gravimetric uptake of an alloy versus the T_{onset} of the first desorption event, where T_{onset} is calculated using Equation (4) [32], with the US DOE target range highlighted. Where the yellow diamonds represent HEAs and intermetallic compounds analysed for hydrogen uptake, and the blue triangles being the hydrides of Mg (T_{onset} = 300 °C, gravimetric uptake = 7.64 wt%), TiFe (T_{onset} = 28.1 °C, gravimetric uptake = 0.90 wt%), Pd (T_{onset} = 150 °C, gravimetric uptake = 0.754 wt%) and $LaNi_5$ (T_{onset} = 100 °C, gravimetric uptake = 1.55 wt%). The values for gravimetric uptake of the HEAs and intermetallic compounds can be found in Table 1, and the values for T_{onset} were calculated using Equation (4). (For interpretation of the references to color/colour in this figure legend, the reader is referred to the Web version of this article.)

Table 8 – Hydrogen affinity (heats of formation model) [62], *VEC* [32], and mass of Mn, Ni, and Zn [74].

Metal	ΔH_∞ (kJ mol^{-1})	ΔH_f (kJ mol^{-1})	VEC [69]	Mass (g mol^{-1})
Mn	1	−8	7	54.94
Ni	10	−3	10	58.70
Zn	15	N/A	12	65.38

Table 9 – Prospective elemental substitution of Cr in the HEA TiZrNbVCr for higher *VEC* elements – Mn, Ni, and Zn – that do not compromise the affinity values of the alloy - and low VEC elements that keep the VEC < 4.75 and improve the hydrogen affinity values. ΔH_∞, ΔH_f, *VEC*, Ω, δ, and T_{onset} for the prospective alloys have been calculated and reported.

Alloy	ΔH_∞ (kJ mol^{-1})	ΔH_f (kJ mol^{-1})	VEC	Ω	δ	T_{onset} (C)
TiZrNbVCr	−28.8	−48.4	4.80	6.40	8.7	319.8
TiZrNbVMn	−34.2	−48.8	5.00	6.05	7.0	283.0
TiZrNbVNi	−32.4	−47.8	5.60	1.35	8.6	172.6
TiZrNbVZn	−31.4	−47.2	6.00	4.62	6.5	99.0
TiZrNbVSc	−52.4	−67.2	4.20	5.01	14.7	430.2
TiZrNbVY	−50.2	−65.4	4.20	2.57	11.0	430.2

increase in gravimetric uptake to within the DOE target range. For example, were the hypothetical quaternary alloy ScTiVZr to have $H/M = 2$, the gravimetric uptake would be 3.32 wt%, however increasing this to $H/M = 3$, the gravimetric uptake could be as high as 4.90 wt% - within the DOE target range. As another example, for the previously synthesised $(TiVNb)_{0.65}Cr_{0.35}$, improving the molar uptake to 3 from 1.7 would offer a gravimetric uptake of 4.82 wt%, and likewise would move closer to the target range of the DOE.

To explain the simultaneous occupation of octahedral and tetrahedral interstitial sites by hydrogen in an FCC lattice, Hu et al. suggested it is driven by the delocalisation of electron density of the hydrogen atom [76]. In metal hydrides of early transition metals, hydrogen acquires electron charge density from the surrounding metal atoms, which Hu et al. attribute to be mainly due to the electronegativity of hydrogen being larger than any A-type transition metal [76] – with hydrogen at $\chi = 2.20$ for H versus $\chi = 1.54$, 1.63, and 1.60 for Ti, V, and Nb respectively [77].

Relative to the hydrides of transition metal elements and traditional alloys where electron density localises homogenously between the hydrogen atoms [76], the computational models formulated by Hu et al. suggest that the electron density of an HEA is less homogenously distributed [76]. For the hydride of TiVZrNb, there are multiple interactions through which electron density may be donated from metal to hydrogen *i.e.*, Ti–H, V–H, Zr–H, Nb–H, at any one time, with varying magnitudes, leading to a complex chemical environment [76]. Moreover, electron localisation function (ELF) calculations conducted by Hu et al. in this work suggest that the electron density in the inter-hydrogen voids reduces, allowing for an increase in electron density localising around the octahedral sites [76]. The polarisation of the hydrogen atom is more achievable with this increased donation, granting the simultaneous occupation of the octahedral and tetrahedral sites [76].

One important observation of HEAs is that they have shown an increase in the stability of cycling hydrogen uptake and release, in some cases. Comparing the variation in uptakes of hydrogen in the quaternary alloy $Ti_{0.325}V_{0.275}Zr_{0.125}Nb_{0.275}$ and the quinary alloy $Mg_{0.1}Ti_{0.3}V_{0.25}Zr_{0.1}Nb_{0.25}$ over the same number of cycles, Montero et al. have shown that by incorporating Mg into an HEA, the intrinsic factors of fading capacity

Please cite this article as: Keith A et al., Perspective of interstitial hydrides of high-entropy alloys for vehicular hydrogen storage, International Journal of Hydrogen Energy, https://doi.org/10.1016/j.ijhydene.2023.01.141

during cycling were reduced [78]. This decrease is often attributed to the disproportionation *via* the emergence of the thermodynamically stable elemental hydrides, *e.g.* ZrH_2 instead of $Ti_{0.3}V_{0.25}Zr_{0.1}Nb_{0.25}H_x$, in the structure over time [78]. This is considered to be potentially due to the randomness of atomic distribution allowing for these separate phases to appear [78]. The hypothesised reasoning for this is that the inclusion of Mg within the alloy offers an improvement in kinetics of absorption and desorption of hydrogen, due to the randomness of elemental distribution for the quinary alloy [78]. Therefore, there appears yet to be another potential advantage in maintaining a high degree of randomness of elemental distribution, which in turn allows for good cycling stability on repeated absorption and desorption. It should be noted that this behaviour requires more research into the ideal configurations and degree of randomness that maximise this stability. All of which could prove very advantageous for the prospect of maintaining reliable storage capacities after multiple cycles, which is especially relevant in the transportation sector.

However, for any solution of a problem to be worth considering, it must be practical and affordable. Therefore, producing these alloys from affordable and abundant metals is not only desirable, but also a necessity. Looking at the potential constituent metal candidates that offer a high hydrogen affinity and are not financially prohibitive (Table 10) can help offer perspective on which candidate metals are viable for deployment in these systems on a large scale – including the *A*-type metals and the above intermediate, high *VEC* metals Mn, Ni, and Zn as they are also prospective components for these alloys.

As highlighted above, there are some metal candidates with a fantastic hydrogen affinity that are logistically infeasible to utilise, *e.g.* Sc, and Hf, due to cost and scarcity. However, metals such as Ti, and Zr, could prove instrumental from an economic perspective for the deployment of these alloys in large scale applications.

Table 10 – Ideal candidate elements for hydride formation in HEAs, their respective *VEC* [69], affinity values based on the Griessen and Driessen Model [63], cost (in GBP) [79], and supply risk [80].

Element	VEC	ΔH_∞ (kJ mol^{-1})	ΔH_f (kJ mol^{-1})	Cost/kg (GBP kg^{-1}) [79]	Supply Risk [80]
Li	1	−51	−97	£92.62	High
Na	1	2	−56	£2.43	Low
Mg	2	27	−37	£1.81	High
K	1	N/A	−58	£10.42	Low
Ca	2	N/A	−94	£4.75	Moderate
Sc	3	−90	−100	£12,009.00	High
Ti	4	−52	−68	£3.02	Low
V	5	−30	−42	£18.09	High
Y	3	−79	−91	£28.02	High
Zr	4	−52	−82	£18.53	Moderate
Nb	5	−38	−44	£33.63	High
La	3	−67	−97	£5.60	High
Hf	4	−38	−66	£1132.00	No Data
Ta	5	−36	−38	£190.50	High
Mn	7	1	−8	£1.65	Moderate
Ni	10	10	−3	£7.36	Moderate
Zn	12	15	N/A	£2.27	Low

Conclusions

Utilising chemical-based, hydrogen-storage materials offers some improvements from a volumetric perspective, and the storage means with the best potential lies in the interstitial hydrides of HEAs. The findings of this work are that these alloys offer a substantial improvement in both the volumetric and gravimetric uptake of hydrogen relative to previously investigated interstitial hydrides. These uptakes are further elevated when adhering to four key considerations: the preferential formation of a BCC alloy, which distorts into a (*pseudo*-)FCC hydride, *VEC*, randomness of the distribution of the elements in the solution, and most crucially, the hydrogen affinity.

Currently the maximum molar and gravimetric uptakes are $H/M = 2.50$ for TiVNbZrHf and 3.05 wt% for TiVNbCr respectively. Improving these uptakes to within the first milestone of the US DOE storage targets of 4.5 wt% and 0.030 g cm^{-3}, and ultimately to 6.5 wt% and 0.050 g cm^{-3}, could potentially be achieved. Due to the prospect of incorporating lightweight elements into these alloys, such approach could prove very useful in on-board vehicular hydrogen storage.

Though the green future of hydrogen very much depends on greener hydrogen gas production, and a well-equipped and functional infrastructure for distribution, introducing hydrogen-powered fuel-cell vehicles should be considered alongside the on-going transition towards BEVs from FFICVs. Utilising HEA hydrides in heavy-duty applications could prove the vital key in reducing and ultimately removing CO_2 emissions from the transportation sector, in the short term, while the production of green hydrogen progresses and becomes more economically advantageous thus making the hydrogen economy a reality.

Declaration of competing interest

The authors declare that they have no known competing financial interests or personal relationships that could have appeared to influence the work reported in this paper.

Acknowledgements

The authors acknowledge funding from the Defence Science and Technology Laboratory, DSTLX1000160445R.

Appendix A. Supplementary data

Supplementary data to this article can be found online at https://doi.org/10.1016/j.ijhydene.2023.01.141.

REFERENCES

[1] European C, Joint Research C, Olivier J, Guizzardi D, Schaaf E, Solazzo E, et al. GHG emissions of all world : 2021 report. Publications Office; 2021.

[2] Seymour Millen EP. In: Transport Df, editor. Transport and environment statistics 2021 annual report; 2021. p. 11.
[3] Waite C. 2019 UK greenhouse gas emissions, final figures. In: Department for business EaIS, editor. Office of national statistics: office of national statistics; 2021. p. 13–5.
[4] Agency EE. In: Agency EE, editor. Greenhouse gas emissions from transport. EEA; 2021.
[5] Thomas CE. Fuel cell and battery electric vehicles compared. Int J Hydrogen Energy 2009;34:6005–20.
[6] Udo Energy. DOE technical targets for Onboard hydrogen storage for light-duty vehicles. In: DOE U; 2021.
[7] Mazloomi K, Gomes C. Hydrogen as an energy carrier: Prospects and challenges. Renew Sustain Energy Rev 2012;16:3024–33.
[8] Energy OoEEaR. Hydrogen Storage. https://www.energy.gov/eere/fuelcells/hydrogen-storage2022..
[9] Sun Z, Lu X, Nyahuma FM, Yan N, Xiao J, Su S, et al. Enhancing hydrogen storage properties of MgH2 by transition metals and Carbon materials: a Brief review. Front Chem 2020;8.
[10] Wan Z, Tao Y, Shao J, Zhang Y, You H. Ammonia as an effective hydrogen carrier and a clean fuel for solid oxide fuel cells. Energy Convers Manag 2021;228:113729.
[11] Efficiency OoEaR. Hydrogen Storage. Hydrogen and fuel cell technologies office.
[12] Johansson M, Skúlason E, Nielsen G, Murphy S, Nielsen RM, Chorkendorff I. Hydrogen adsorption on palladium and palladium hydride at 1bar. Surf Sci 2010;604:718–29.
[13] Schlapbach L. Hydrogen in intermetallic compounds I. Berlin, Germany: Springer Verlag; 1988.
[14] Tousignant M, Huot J. Hydrogen sorption enhancement in cold rolled LaNi5. J Alloys Compd 2014;595:22–7.
[15] Bosko ML, Dalla Fontana A, Tarditi A, Cornaglia L. Advances in hydrogen selective membranes based on palladium ternary alloys. Int J Hydrogen Energy 2021;46:15572–94.
[16] Martin D. Thermodynamics of metal hydrides: tailoring reaction Enthalpies of hydrogen storage materials. In: Juan Carlos M-P, editor. Thermodynamics. Rijeka: IntechOpen; 2011. Ch. 33.
[17] Zlotea C, Sow MA, Ek G, Couzinié JP, Perrière L, Guillot I, et al. Hydrogen sorption in TiZrNbHfTa high entropy alloy. J Alloys Compd 2019;775:667–74.
[18] Tsai M-H, Yeh J-W. High-entropy alloys: a critical review. Materials Research Letters 2014;2:107–23.
[19] Ma H, Shek CH. Effects of Hf on the microstructure and mechanical properties of CoCrFeNi high entropy alloy. J Alloys Compd 2020;827:154159.
[20] Long Y, Liang X, Su K, Peng H, Li X. A fine-grained NbMoTaWVCr refractory high-entropy alloy with ultra-high strength: Microstructural evolution and mechanical properties. J Alloys Compd 2019;780:607–17.
[21] Shi Y, Yang B, Liaw PK. Corrosion-resistant high-entropy alloys: a review. Metals 2017;7:43.
[22] Baker I. Interstitials in f.c.c. High Entropy Alloys. Metals 2020;10:695.
[23] Fortulan R, Aminorroaya Yamini S, Nwanebu C, Li S, Baba T, Reece MJ, et al. Thermoelectric performance of n-type Magnetic element Doped Bi2S3. ACS Appl Energy Mater 2022;5:3845–53.
[24] Li H, Lai J, Li Z, Wang L. Multi-sites electrocatalysis in high-entropy alloys. Adv Funct Mater 2021;31:2106715.
[25] Mohammadi A, Ikeda Y, Edalati P, Mito M, Grabowski B, Li H-W, et al. High-entropy hydrides for fast and reversible hydrogen storage at room temperature: Binding-energy engineering via first-principles calculations and experiments. Acta Mater 2022;236:118117.
[26] Sahlberg M, Karlsson D, Zlotea C, Jansson U. Superior hydrogen storage in high entropy alloys. Sci Rep 2016;6:36770.
[27] Park KB, Park J-Y, Kim YD, Choi J-I, Im H-T, Kang J-W, et al. Study on hydrogen absorption and surface properties of TiZrVNbCr high entropy alloy. Intermetallics 2021;130:107074.
[28] Joubert J-M, Paul-Boncour V, Cuevas F, Zhang J, Latroche M. LaNi5 related AB5 compounds: structure, properties and applications. J Alloys Compd 2021;862:158163.
[29] Bellosta von Colbe J, Ares J-R, Barale J, Baricco M, Buckley C, Capurso G, et al. Application of hydrides in hydrogen storage and compression: Achievements, outlook and perspectives. Int J Hydrogen Energy 2019;44:7780–808.
[30] Kunce I, Polanski M, Bystrzycki J. Structure and hydrogen storage properties of a high entropy ZrTiVCrFeNi alloy synthesized using Laser Engineered Net Shaping (LENS). Int J Hydrogen Energy 2013;38:12180–9.
[31] Kunce I, Polanski M, Bystrzycki J. Microstructure and hydrogen storage properties of a TiZrNbMoV high entropy alloy synthesized using Laser Engineered Net Shaping (LENS). Int J Hydrogen Energy 2014;39:9904–10.
[32] Nygård MM, Ek G, Karlsson D, Sørby MH, Sahlberg M, Hauback BC. Counting electrons - a new approach to tailor the hydrogen sorption properties of high-entropy alloys. Acta Mater 2019;175:121–9.
[33] Montero J, Zlotea C, Ek G, Crivello J-C, Laversenne L, Sahlberg M. TiVZrNb multi-Principal-element alloy: synthesis Optimization, structural, and hydrogen sorption properties. Molecules 2019;24:2799.
[34] Spaliviero UPMG, Battezzati L, Baricco M. Hydrogen sorption in TiV0.6Cr0.3Zr0.3NbMo high Entopy alloy. La Metall Ital 2019;6.
[35] Nygård MM, Ek G, Karlsson D, Sahlberg M, Sørby MH, Hauback BC. Hydrogen storage in high-entropy alloys with varying degree of local lattice strain. Int J Hydrogen Energy 2019;44:29140–9.
[36] Shen H, Hu J, Li P, Huang G, Zhang J, Zhang J, et al. Compositional dependence of hydrogenation performance of Ti-Zr-Hf-Mo-Nb high-entropy alloys for hydrogen/tritium storage. J Mater Sci Technol 2020;55:116–25.
[37] de Marco MO, Li Y, Li H-W, Edalati K, Floriano R. Mechanical synthesis and hydrogen storage characterization of MgVCr and MgVTiCrFe high-entropy alloy. Adv Eng Mater 2020;22:1901079.
[38] Zhang C, Song A, Yuan Y, Wu Y, Zhang P, Lu Z, et al. Study on the hydrogen storage properties of a TiZrNbTa high entropy alloy. Int J Hydrogen Energy 2020;45:5367–74.
[39] Edalati P, Floriano R, Mohammadi A, Li Y, Zepon G, Li H-W, et al. Reversible room temperature hydrogen storage in high-entropy alloy TiZrCrMnFeNi. Scripta Mater 2020;178:387–90.
[40] Dewangan SK, Sharma VK, Sahu P, Kumar V. Synthesis and characterization of hydrogenated novel AlCrFeMnNiW high entropy alloy. Int J Hydrogen Energy 2020;45:16984–91.
[41] Ek G, Nygård MM, Pavan AF, Montero J, Henry PF, Sørby MH, et al. Elucidating the effects of the composition on hydrogen sorption in TiVZrNbHf-based high-entropy alloys. Inorg Chem 2021;60:1124–32.
[42] Strozi RB, Leiva DR, Huot J, Botta WJ, Zepon G. Synthesis and hydrogen storage behavior of Mg–V–Al–Cr–Ni high entropy alloys. Int J Hydrogen Energy 2021;46:2351–61.
[43] Montero J, Ek G, Sahlberg M, Zlotea C. Improving the hydrogen cycling properties by Mg addition in Ti-V-Zr-Nb refractory high entropy alloy. Scripta Mater 2021;194:113699.
[44] Cardoso KR, Roche V, Jorge Jr AM, Antiqueira FJ, Zepon G, Champion Y. Hydrogen storage in MgAlTiFeNi high entropy alloy. J Alloys Compd 2021;858:158357.
[45] Zhang J, Li P, Huang G, Zhang W, Hu J, Xiao H, et al. Superior hydrogen sorption kinetics of Ti0.20Zr0.20Hf0.20Nb0.40 high-entropy alloy, vol. 11. Metals; 2021.
[46] Strozi RB, Leiva DR, Zepon G, Botta WJ, Huot J. Effects of the Chromium content in (TiVNb)100−xCrx Body-Centered cubic

Please cite this article as: Keith A et al., Perspective of interstitial hydrides of high-entropy alloys for vehicular hydrogen storage, International Journal of Hydrogen Energy, https://doi.org/10.1016/j.ijhydene.2023.01.141

high entropy alloys designed for hydrogen storage applications. Energies 2021:14.
[47] Silva BH, Zlotea C, Champion Y, Botta WJ, Zepon G. Design of TiVNb-(Cr, Ni or Co) multicomponent alloys with the same valence electron concentration for hydrogen storage. J Alloys Compd 2021;865:158767.
[48] Strozi RB, Leiva DR, Huot J, Botta WJ, Zepon G. An approach to design single BCC Mg-containing high entropy alloys for hydrogen storage applications. Int J Hydrogen Energy 2021;46:25555–61.
[49] Floriano R, Zepon G, Edalati K, Fontana GLBG, Mohammadi A, Ma Z, et al. Hydrogen storage properties of new A3B2-type TiZrNbCrFe high-entropy alloy. Int J Hydrogen Energy 2021;46:23757–66.
[50] Park KB, Park J-Y, Kim YD, Fadonougbo JO, Kim S, Kim H-K, et al. Characterizations of hydrogen absorption and surface properties of Ti0.2Zr0.2Nb0.2V0.2Cr0.17Fe0.03 high entropy alloy with dual phases. Mater Charact 2022;186:111767.
[51] Sarac B, Zadorozhnyy V, Ivanov YP, Spieckermann F, Klyamkin S, Berdonosova E, et al. Transition metal-based high entropy alloy microfiber electrodes: corrosion behavior and hydrogen activity. Corrosion Sci 2021;193:109880.
[52] Ma X, Ding X, Chen R, Cao W, Song Q. Study on hydrogen storage property of (ZrTiVFe)xAly high-entropy alloys by modifying Al content. Int J Hydrogen Energy 2022;47:8409–18.
[53] Fukagawa T, Saito Y, Matsuyama A. Effect of varying Ni content on hydrogen absorption–desorption and electrochemical properties of Zr-Ti-Ni-Cr-Mn high-entropy alloys. J Alloys Compd 2022;896:163118.
[54] Zepon G, Leiva DR, Strozi RB, Bedoch A, Figueroa SJA, Ishikawa TT, et al. Hydrogen-induced phase transition of MgZrTiFe0.5Co0.5Ni0.5 high entropy alloy. Int J Hydrogen Energy 2018;43:1702–8.
[55] Hu J, Zhang J, Xiao H, Xie L, Sun G, Shen H, et al. A first-principles study of hydrogen storage of high entropy alloy TiZrVMoNb. Int J Hydrogen Energy 2021;46:21050–8.
[56] Hu J, Shen H, Jiang M, Gong H, Xiao H, Liu Z, et al. A DFT study of hydrogen storage in high-entropy alloy TiZrHfScMo. Nanomaterials 2019;9:461.
[57] Jiang DE, Carter EA. Diffusion of interstitial hydrogen into and through bcc Fe from first principles. Phys Rev B 2004;70:064102.
[58] Bodega J, Fernández JF, Leardini F, Ares JR, Sánchez C. Synthesis of hexagonal C14/C36 and cubic C15 ZrCr2 Laves phases and thermodynamic stability of their hydrides. J Phys Chem Solid 2011;72:1334–42.
[59] Westlake DG. Stoichiometries and interstitial site occupation in the hydrides of zrni and other isostructural intermetallic compounds. J Less Common Met 1980;75:177–85.
[60] Rao BK, Jena P. Switendick criterion for stable hydrides. Phys Rev B 1985;31:6726–30.
[61] Borgschulte A, Terreni J, Billeter E, Daemen L, Cheng Y, Pandey A, et al. Inelastic neutron scattering evidence for anomalous H–H distances in metal hydrides. Proc Natl Acad Sci USA 2020;117:4021–6.
[62] Driessen G. Heat of formation models. Berlin, Heidelberg: Springer; 1988.
[63] Percheron-Guégan AWJ. Preparation of intermetallics and hydrides. Berlin, Germany: Springer; 1988.
[64] Galey B, Auroux A, Sabo-Etienne S, Dhaher S, Grellier M, Postole G. Improved hydrogen storage properties of Mg/MgH2 thanks to the addition of nickel hydride complex precursors. Int J Hydrogen Energy 2019;44:28848–62.
[65] Schnitzler S, Spaniol TP, Okuda J. Reactivity of a molecular Magnesium hydride featuring a terminal Magnesium–hydrogen bond. Inorg Chem 2016;55:12997–3006.
[66] Filinchuk YE, Yvon K. Directional metal–hydrogen bonding in interstitial hydrides. III. Structural study of ErCo3Dx (0⩽x⩽4.3). J Solid State Chem 2006;179:1041–52.
[67] von Rohr F, Winiarski MJ, Tao J, Klimczuk T, Cava RJ. Effect of electron count and chemical complexity in the Ta-Nb-Hf-Zr-Ti high-entropy alloy superconductor. Proc Natl Acad Sci USA 2016;113:E7144–50.
[68] Guo S, Ng C, Lu J, Liu CT. Effect of valence electron concentration on stability of fcc or bcc phase in high entropy alloys. J Appl Phys 2011;109:103505.
[69] Miracle DB, Senkov ON. A critical review of high entropy alloys and related concepts. Acta Mater 2017;122:448–511.
[70] Mansoori GA, Carnahan NF, Starling Jr KE. TWL. Equilibrium thermodynamic properties of the mixture of hard spheres. J Chem Phys 1971;54:1523–5.
[71] Ye YF, Wang Q, Lu J, Liu CT, Yang Y. Design of high entropy alloys: a single-parameter thermodynamic rule. Scripta Mater 2015;104:53–5.
[72] Yang X, Zhang Y. Prediction of high-entropy stabilized solid-solution in multi-component alloys. Mater Chem Phys 2012;132:233–8.
[73] Ye YF, Wang Q, Lu J, Liu CT, Yang Y. The generalized thermodynamic rule for phase selection in multicomponent alloys. Intermetallics 2015;59:75–80.
[74] angelo.edu. Atomic Masses 2022.
[75] UoN Texas. Interstitial sites. 2019.
[76] Hu J, Zhang J, Li M, Zhang S, Xiao H, Xie L, et al. The origin of anomalous hydrogen occupation in high entropy alloys. J Mater Chem 2022;10:7228–37.
[77] Aboud S, Wilcox J. A density functional theory study of the charge state of hydrogen in metal hydrides. J Phys Chem C 2010;114:10978–85.
[78] Montero J, Ek G, Sahlberg M, Zlotea C. Improving the hydrogen cycling properties by Mg addition in Ti-V-Zr-Nb refractory high entropy alloy. Scripta Mater 2021.
[79] leonlandde Chemical elements by market price. leonland.de..
[80] Rso Chemistry. Periodic table. Royal Society of Chemistry; 2022. https://www.rsc.org/periodic-table.

Please cite this article as: Keith A et al., Perspective of interstitial hydrides of high-entropy alloys for vehicular hydrogen storage, International Journal of Hydrogen Energy, https://doi.org/10.1016/j.ijhydene.2023.01.141